Chapter 2
Microstructure

The Si-based light emitters to be discussed in this book are based on an RE-implanted, standard MOS structure with an additional dielectric layer, also known from MNOS (metal–nitride–oxide–semiconductor) devices. There is a giant pool of literature about Si technology, Si processing, the structure and point defects in SiO_2 and related materials, as well as about the structural properties of the Si–SiO_2 interface. Consequently, Sect. 2.1 reports only on the specific fabrication and device parameters used for the light emitter preparation. Section 2.2 touches briefly on the topic of point defects in SiO_2 and SiON as well as the issue of RE diffusion under annealing, while Sect. 2.3 concentrates on the formation and the evolution of clusters.

2.1 Device Structure and Fabrication

2.1.1 Layout

Usually, the Si-based light emitters are prepared by standard silicon MOS technology and consist of a layer stack with Si substrate at the bottom, followed by a thermally grown gate oxide, a SiON layer deposited by PECVD and a transparent front electrode made of ITO. Although the gate oxide is the active medium that contains the RE LCs, the SiON layer is a dielectric protection layer, which strongly enhances the operation lifetime of the devices [142, 148]. The latter point is comprehensively discussed in Sect. 6.3. Generally, a gate oxide thickness of 100 nm is used, although for some specific investigations, a 200-nm thick SiO_2 layer or thinner layers with a thickness ranging between 10 and 75 nm were used. Typical SiON layer thicknesses range from 50 to 200 nm but amount to 100 nm in most cases. If the light emitter is intended to be used in humid or wet media, the device can be passivated by a thick SiO_2 layer deposited by PECVD, which leaves only the contact pads open. The rear electrode made of aluminium is fabricated on the backside of the Si wafer. In the following sections, such a structure is called MOS light emitting device (MOSLED).

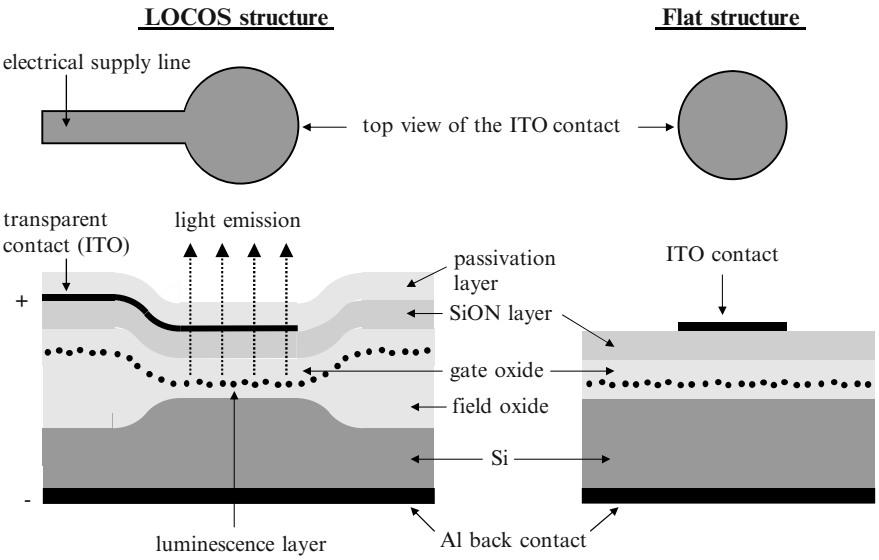

Fig. 2.1 Basic designs of RE-implanted MOSLEDs in the form of a LOCOS structure (*left*) or a flat structure (*right*) together with a *top view of the upper supply line*

As shown in Fig. 2.1, the light emitters were fabricated using two different designs. The more complex structure is processed in local oxidation of silicon (LOCOS) technology, (see [149, 150] for more details) with the gate oxide being surrounded by a thicker field oxide. This design allows the processing of electrical supply lines together with the upper ITO electrode as applying a voltage between the upper and lower electrodes would result in a larger electric field across the thin gate oxide than across the thick field oxide. As a result, only the gate oxide area emits light and not the area of the electrical supply line. In addition, the bird beak-shaped transition between the field and gate oxide avoids an early electrical breakdown at the edge of the electrode and thus prolongs, together with the SiON layer, the operation lifetime of the devices. Because of these advantages, the LOCOS design of the light emitters is usually applied in real applications. However, the LOCOS design is troublesome for a couple of electrical and microstructural investigations. If the capacitance of the MOS structure has to be measured, the signal is always composed of the component of the light emitting area and the contribution of the electrical supply line. In case of microstructural investigations such as TEM, RBS and AES, advanced preparation techniques (e.g. focused ion beam preparation) are required to hit the light emitter area precisely. Sometimes even the ITO electrode is perturbing, e.g. for RBS because of mass interferences between indium and the RE elements. For such investigations, a flat structure is used, as schematically drawn on the right of Fig. 2.1.

The fabrication of the light emitters starts with the LOCOS process, including the thermal growth of the gate oxide by dry oxidation at 1,050°C, followed by ion

implantation of RE elements and a thermal treatment. The details of the implantation and the thermal treatment are discussed in the subsequent chapters. The processing is continued with the deposition of a SiON layer by PECVD at a temperature of 325°C, followed by exactly the same thermal treatment performed after the ion implantation. All the implications connected with implantation-induced defects in SiO_2 and the hydrogen load of SiON are discussed in Sects. 2.2.1 and 2.2.2, respectively. After the second thermal treatment, the Al back electrode is sputtered in combination with a contact annealing at 400°C, followed by magnetron sputtering of ITO on the front side of the wafer. It is worth noting that the use of Si_3N_4 instead of SiON may cause adhesion problems of the ITO layer. The upper electrode is structured by means of lithographic patterning, whereas the size, the shape and the arrangement of the light emitters are only limited by the possibilities of photolithography. If not otherwise stated, the electrical and optical results presented in this work were obtained from circular dots with a diameter of 300 μm, although feature sizes down to 2 μm were tested. Figure 2.2 gives a brief impression of what is technically feasible.

2.1.2 Rare Earth Implantation

Ion implantation is an essential processing step that determines the special type of light emitter by the RE element and influences the operation lifetime and efficiency by the implantation dose. The RE ions, namely the elements Ce, Pr, Eu, Gd, Tb, Er

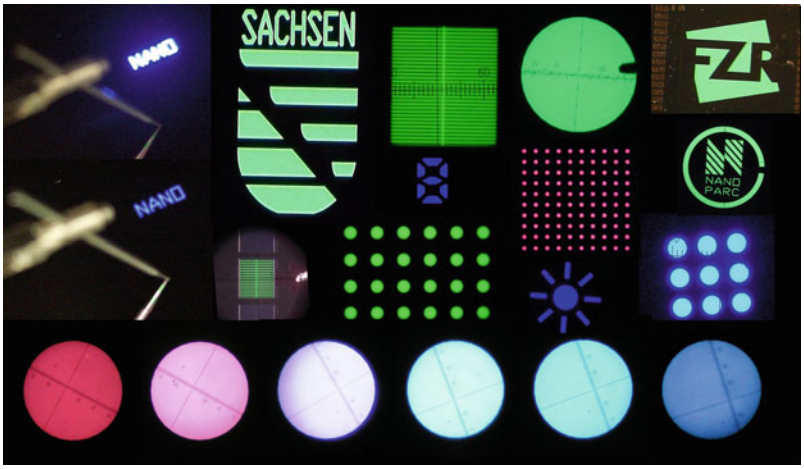

Fig. 2.2 Light emitting Ge- and RE-implanted MOS structures with different layouts. The *blue*, *green* and *reddish* structures in the *upper part of the figure* originate from Ge-, Tb- and Gd-implanted MOSLEDs. The *lower row* displays Eu-implanted MOSLEDs, with different Eu concentrations processed under different annealing conditions

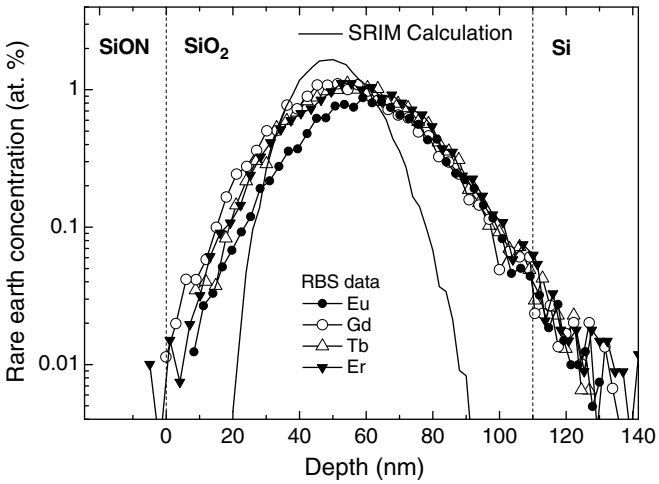

Fig. 2.3 Elemental depth profiles calculated for 100 keV Tb by SRIM (*solid line*) and profiles calculated from RBS spectra for Eu, Gd, Tb and Er in SiO_2 implanted with a nominal dose of $3 \times 10^{15}\,cm^{-2}$. The nominal peak concentration of Tb was 1.5%

and Yb, were single implanted in such a way that the projected range of implantation R_P is approximately in the middle of the gate oxide layer, which corresponds to an implantation energy of about 100 keV for an oxide thickness of 100 nm. Some attention should be paid to the fact that not too many ions are implanted into the Si–SiO_2 interface so as to keep its excellent electrical quality. In addition, RE ions that are located too close to the injecting interface will not take part in the electrical excitation process as outlined in Sect. 5.2.2. According to SRIM calculations [151], the depth profile has a Gaussian-like shape with a slight asymmetry as shown in Fig. 2.3. The implantation dose was varied according to the desired peak concentration of the implanted ions, which ranged from 0.25 to 9%. Optimum results were mostly achieved for RE concentrations between 1 and 3%.

However, there are already slight differences in the as-implanted profile between the prediction of SRIM and the profiles calculated from RBS spectra. As shown in Fig. 2.3, the RBS profiles are significantly broader, and this is accompanied by an adequate reduction of the peak concentration. Furthermore, the total dose of implanted ions as calculated from RBS spectra deviates in the order of 10% from the nominal value of $3 \times 10^{15}\,cm^{-2}$. In detail, total doses of $2.65 \times 10^{15}\,cm^{-2}$, $3.44 \times 10^{15}\,cm^{-2}$, $3.33 \times 10^{15}\,cm^{-2}$ and $3.46 \times 10^{15}\,cm^{-2}$ were measured for Eu, Gd, Tb and Er, respectively. This is most probably due to the implantation-induced diffusion processes that may occur under high implantation currents. Nevertheless, the value of the nominal peak concentration is used in the following to avoid confusion.

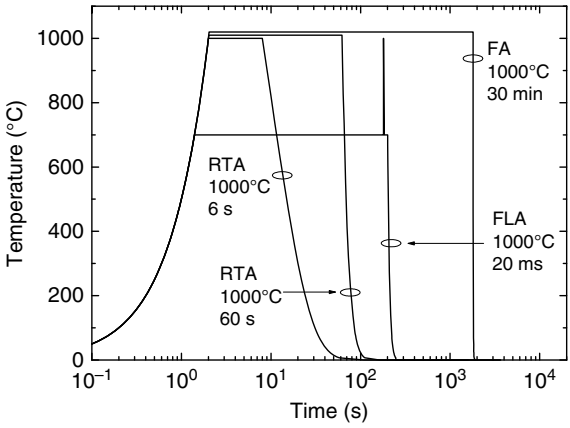

Fig. 2.4 Schematic temperature profiles of different types of annealing. The plateau at 1,000°C is slightly split for better projection

2.1.3 Annealing Conditions

Appropriate choice of annealing conditions strongly determines the operation lifetime and efficiency of the potential light emitter. On the one side, annealing is necessary to remove implantation-induced defects, to anneal defects introduced by the PECVD deposition and to activate the RE LCs. On the other, large-scale redistributions such as diffusion or the formation of huge clusters have to be avoided. The RE-implanted MOSLEDs were subjected to several types of annealing, namely furnace annealing (FA), rapid thermal annealing (RTA) and flash lamp annealing (FLA), which cover a wide range of annealing times. Figure 2.4 shows the schematic temperature profiles of the different types of annealing with an arbitrary ramp and cooling phase in order to illustrate the different physical meanings of the annealing times. For the RE-implanted MOSLEDs discussed in this book, mainly five types of annealing were used, but with different annealing temperatures: FA for 30 min, RTA for 6 or 60 s and FLA for 0.6 or 20 ms. Although for FA 30 min and RTA 60 s, the ramp and cooling phase is negligible, for RTA 6 s it forms a significant part of the temperature profile. The temperature load is therefore higher than in the ideal case of a rectangular profile. This point is even more critical in the case of FLA. First, a preheating, lasting several minutes (at 700°C for 3 min in our case), is usually applied before the flash is added. Second, the annealing time of 0.6 and 20 ms denotes the width of the applied flash pulse, but the cooling occurs, obviously, on a much longer time scale. Nevertheless, the thermal budget applied to a sample declines undoubtedly with decreasing annealing time, but possibly not exactly by the factor the different annealing times imply. Further information about RTA and FLA technology can be found in [152, 153]. As already mentioned in Sect. 2.1.1, a specific type of annealing was always applied twice to the light emitters.

The term "thermal budget" denotes a certain combination of annealing time and annealing temperature, but is not exactly defined in the literature. Two thermal budgets with temperatures T_1 and T_2 as well as annealing times t_1 and t_2 can easily be

compared if both relations $T_1 > T_2$ and $t_1 > t_2$ are valid or vice versa. However, combinations such as $T_1 > T_2$ and $t_1 < t_2$ are much more problematic. A simple, traditional definition for the thermal budget is the product of time and temperature, or more generally, the area under the curves in Fig. 2.4. However, this definition is impractical in most cases as, for example, the effect of an annealing with $T_1 = 400\,\mathrm{K}$ and $t_1 = 4$ min is hardly the same as that with $T_1 = 1{,}600\,\mathrm{K}$ and $t_1 = 1$ min. It is therefore more reasonable to define the thermal budget according to the physical effect the application of a certain thermal budget will cause. Assuming that the effect of annealing temperature and time is similar to the case of diffusion, the thermal budget might be proportional to $\sqrt{t_i}\exp(-E_\mathrm{a}/kT_i)$, with E_a being general activation energy. If the ratio between two thermal budgets is used to decide which one is higher, the result will depend on the specific value of E_a. Because of this ambiguity, further discussion on thermal budgets is conducted qualitatively, which is, however, sufficient to outline the main tendencies of the behaviour of RE-implanted MOSLEDs. A more detailed discussion about thermal budgets for short-time annealing can be found in [154, 155].

2.2 Point Defects and Diffusion

2.2.1 Intrinsic and Implantation Induced Defects in SiO_2

SiO_2 as the most essential dielectric in microelectronics and its interface to Si is one of the best investigated material. There have been numerous surveys of the structure and point defects of amorphous SiO_2 [156–162]. Shortly, amorphous SiO_2 consists of tetrahedron rings with a Si atom in the centre and four oxygen atoms at the corners of the tetrahedron. The number of tetrahedrons in the ring and the angle between two tetrahedrons can range from 3 to 8 and 120° to 180°, respectively, with the most probable value of 6 ring members and 144° for the Si–O–Si bond angle of amorphous SiO_2 [156]. Because of the higher atomic concentration of Si atoms in crystalline Si compared with SiO_2, there is a transition zone extending up to 3 nm from the Si–SiO_2 interface into the SiO_2. Within this zone, tetrahedron rings with 3–4 members dominate, and the concentration of the Si^{3+} suboxide measured by XPS increases towards the interface [156].

Defects in SiO_2 can be generally classified as to whether they are oxygen deficient or excessive in nature [163]. Figure 2.5 displays the ≡Si–O–Si≡ bond in the undisturbed SiO_2 network and possible defects in the oxide matrix. If the bond between one oxygen and one Si atom of the SiO_2 network is broken, the E' centre ≡Si• and the non-bridging oxygen hole centre •O–Si≡ may arise, which are both visible with electron spin resonance measurements, due to the unpaired spin of the single electron. The E' centre, which exists in many modifications depending on its chemical environment [158], is believed to be a precursor of the NOV. Another possibility is the formation of the twofold coordinated Si-atom Si_2^0, which requires

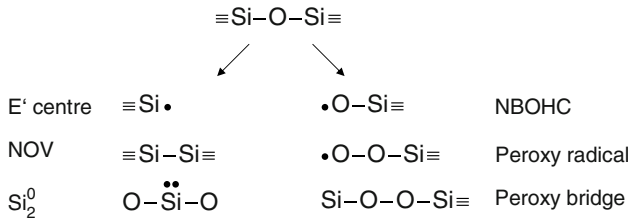

Fig. 2.5 Basic scheme of possible defects in the SiO_2 (after [67] and [163])

the breaking of two Si bonds. By binding an OH group followed by hydrogen dissociation, the non-bridging oxygen hole centre can transform into a peroxy radical or peroxy bridge. In the E' centre, the NOV and Si_2^0 are assigned to the category of ODCs, whereas the NBOHC and the peroxy structures are regarded as oxygen excess defects together with interstitial oxygen in the form of O_2 and ozone. Furthermore, there are additional types of ODCs with more than two Si atoms. Mostly, the defects can convert into each other, and the possible termination of dangling bonds by hydrogen adds another degree of freedom. Finally, small Si nanoclusters can be formed under high temperature annealing.

The SiO_2 network is heavily damaged during the RE implantation. Figure 2.6a shows the energy deposition during a 100 keV Tb implantation with a nominal dose of $3 \times 10^{15}\,\mathrm{cm}^{-2}$, according to the energy transfer of the Tb ions to electrons, phonons and atoms of the target material. The first two processes lead mainly to bond breaking and the heating of the target, while the last process displaces the target atoms. The dashed horizontal line marks the amount of energy deposition that is required to cause maximum damage in amorphous SiO_2 [159, 165] and to amorphize crystalline Si [164]. As seen in Fig. 2.6a, the SiO_2 network is completely destroyed in the front part of the SiO_2 layer, and even the Si close to the Si–SiO_2-interface is exposed to an energy deposition, which is not enough for a complete amorphization but sufficient to cause a significant damage. During the displacement of a target atom, a significant momentum in the forward direction is also transferred to the displaced atom, leading qualitatively to a vacancy and interstitial distribution, as shown in Fig. 2.6b. Although these profiles overestimate the real concentration of vacancies and interstitials because of the partial reconstruction of the SiO_2 network during the implantation process, the qualitative picture is obvious. These profiles demonstrate that there are deviations from the stoichiometric Si:O ratio of SiO_2, implying the existence of regions with a local excess of Si or oxygen and the formation of the corresponding defects. In fact, typical defects found after implantation are the NOVs, E' centres, peroxy radicals and interstitial O_2 [166]. Additionally, this ensemble of defects is extended by defect types caused by the implanted RE ions.

With increasing annealing temperature, the different types of defects are successively annealed out. So the concentration of E' centres measured by ESR decreases with increasing annealing temperature and almost disappears at 600°C [167]. The

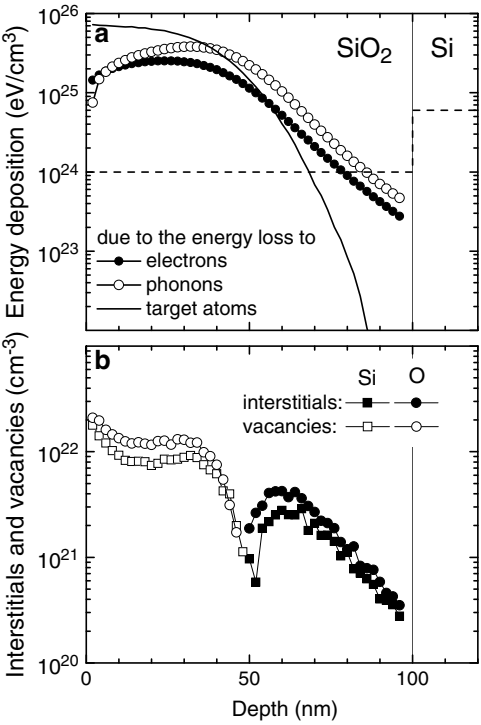

Fig. 2.6 Energy deposition (**a**) and resulting profiles of Si and O interstitials or vacancies (**b**) according to a full damage cascade calculation by SRIM [151] for a 100 keV Tb implantation into 100 nm SiO_2 on Si, with a nominal dose of $3 \times 10^{15}\,cm^{-2}$. The *dashed line* in (**a**) represents the value of energy deposition, which is necessary to amorphize Si [164] or to cause maximum damage in SiO_2 at room temperature [159, 165]

same temperature was needed to anneal out implantation-induced defects, as probed by positron annihilation spectroscopy [168]. However, especially for heavier ions, higher temperatures are needed, which probably have to reach the original growth temperature of the SiO_2 layer for an optimum recovery of the SiO_2 network [165]. In addition, the implanted RE ions introduce a non-stoichiometry and compete with Si for oxygen, for which reason ODCs will remain in the oxide layer even after FA 1,000°C. Furthermore, in case of RE or RE oxide cluster formation, there exists a shell of structural defects around the clusters as they do not fit perfectly into the SiO_2 network.

2.2.2 Hydrogen and Other Defects in SiON

The properties of SiON deposited by PECVD strongly depends on the fabrication conditions, namely on the deposition temperature, the gas flow ratio, the pressure, the HF power and even the geometry of the plasma chamber. Nevertheless, there are some general properties that are briefly discussed in the following section, together with the results of our measurements. Similar to SiO_2, the network of $Si_xN_yH_z$ is also based on Si-centred tetrahedrons, but with N or Si atoms at the corners [169].

As proved by X-ray absorption near-edge spectroscopy, the Si-centred tetrahedron with N or O atoms at the corners is the basic structural element of the network of SiON layers produced by PECVD [170]. There is a significant number of dangling Si or N bonds, which are frequently denoted in the literature as K and N centres, respectively. Because of the variability of the local network structure, there is a large family of different K centre types, as illustrated in [171]. The use of SiH_4 during deposition introduces larger amounts of hydrogen into the layers, which results in a termination of the dangling bonds by hydrogen. In case of SiON, a fraction of the N sites is occupied by oxygen. In addition, oxygen also substitutes hydrogen bonded to Si, which results in a much higher number of N–H bonds compared with the number of Si–H bonds [171]. As in the case of SiO_2, missing oxygen or nitrogen atoms can give rise to the formation of NOV defects [172, 173], whose number, however, is assumed to be low in the case of stoichiometric SiON (i.e. no Si excess).

Clearly, the hydrogen content of a SiON layer deposited by PECVD or LPCVD decreases with higher deposition temperature [174] or with a post-deposition thermal treatment at temperatures above the deposition temperature [175–177], but there is a discussion in the literature on whether this improves the quality of the SiON or not. In some cases, a compaction of the SiON layer with a shrinking of the layer thickness and the danger of crack formation is observed [178]. However, the removal of hydrogen is not accompanied by an adequate increase of N and Si dangling bonds because of the cross linking effect, which leads to the formation of new Si–N bonds, as measured by FTIR absorption spectroscopy [175]. It was reported that the density of paramagnetic defects in SiON traced by electron spin resonance generally decreases with annealing but shows a minimum in the temperature range of 500–600°C [176]. Other investigations revealed that the electrical quality of thin SiON layers improved after RTA 900°C or FA 900°C, in terms of lower interface trap densities and lower leakage currents [179].

Figure 2.7 compares the hydrogen content of unimplanted and Eu-implanted MOSLEDs for different annealing conditions. The hydrogen depth profile was determined by nuclear reaction analysis (NRA), exploiting the resonant reaction $^{15}N\,(6.385\,MeV) + {}^{1}H \rightarrow {}^{12}C + {}^{4}He + \gamma\text{-rays}\ (4.43\,MeV)$ by increasing the incident energy of ^{15}N ions and thus moving the resonance at 6.385 MeV progressively to greater depths. In all the cases, the hydrogen profiles are characterized by a nearly constant concentration in the SiON layer, which drops down at the SiO_2–SiON interface by a factor of 3–10 depending on the type of annealing. In the as-implanted state, a hydrogen concentration of about 18% is measured in the SiON layer, whereas this value decreases to 3% and 0.2% in the case of FLA 1,000°C and FA 1,000°C, respectively. The comparison between Eu-implanted devices (closed symbols) and unimplanted devices (open symbols) reveals that (1) the hydrogen content strongly decreases with an increasing thermal budget, as expected from the literature and (2) that this process is entirely independent of whether the MOSLED was implanted or not.

The loss of hydrogen is accompanied by a compaction of the SiON layer, which was investigated by ellipsometric measurements. Figure 2.8 shows the relative thickness and the refraction index of the SiON layer at a wavelength of 633 nm as a

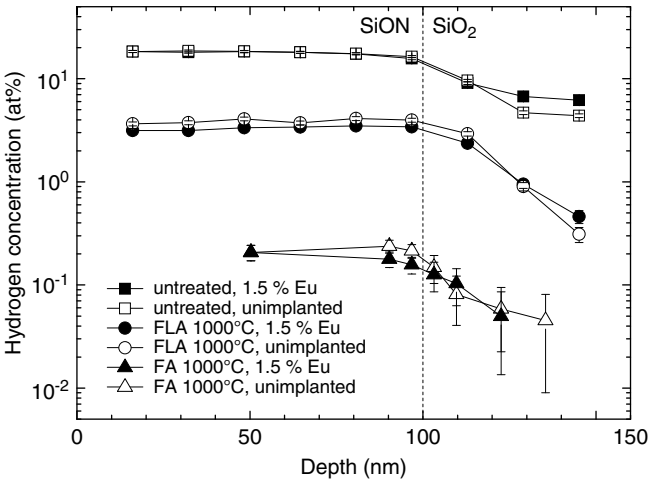

Fig. 2.7 Elemental depth profiles of hydrogen in unimplanted and Eu-implanted MOSLEDs, as derived from NRA. A SiO_2 density of $2.2\,g\,cm^{-3}$ and an average energy loss of $1.55\,keV\,nm^{-1}$ have been assumed to calculate the depth scale (after [132])

function of the annealing time at 1,000°C (a) and the annealing temperature (b). The as-deposited SiON layer shrinks by 13–14% if subjected to FLA 1,000°C 20 ms or FA 700°C, followed by a more shallow decrease of the layer thickness for higher thermal budgets. Concurrently, the refraction index increases from 1.73 to 1.76–1.78, followed by a further increase to 1.82 for higher thermal budgets. In a first approximation, the relative compaction of the SiON layer seems to be independent of the SiON layer thickness. The compaction will give a minor but significant contribution to the interpretation of electrical results, which is discussed in the corresponding chapters.

The composition of the layer system Si–SiO_2–SiON was traced by AES measurements as illustrated in Fig. 2.9. As seen, the SiON layer has a slight excess of nitrogen compared with oxygen, i.e. the relative oxygen ratio R_{Ox}, defined as

$$R_{Ox} = \frac{c_O}{c_O + c_N} \tag{2.1}$$

with c as the atomic concentration of the corresponding element, is about 0.46. On the contrary, the ratio between Si and the elements oxygen and nitrogen is stoichiometric. The SiON compaction is clearly visible due to the reduction of the SiON layer thickness from the original 100 nm down to ∼80 nm. Finally, it should be noted that the deposition of Si_3N_4 and SiON on SiO_2 can lead to Si excess at the SiO_2–SiON interface [181].

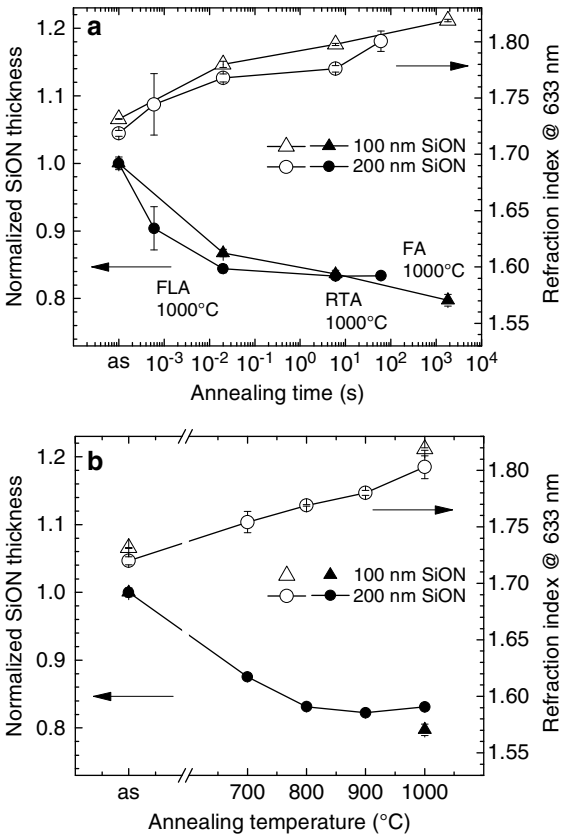

Fig. 2.8 Relative thickness and the refraction index of the SiON layer measured by ellipsometry at 633 nm for different annealing times (**a**) and different annealing temperatures (**b**). The as-deposited SiON is labelled with "as" [180]

2.2.3 Diffusion of Rare Earth Atoms in SiO_2

The redistribution of implanted RE elements under high temperature annealing was investigated by RBS, for the elements Eu, Gd, Tb and Er. These results clearly split the elements into two groups with Eu being in the first and the other elements being in the second group. For the investigated RE elements except Eu, there is little diffusion of RE atoms up to an annealing temperature of 1,000°C. Only for temperatures above 1,000°C, a considerable diffusion of RE atoms towards the interfaces of the SiO_2 layer (Fig. 2.10) can be observed. In addition, the investigation of Gd- and Er-implanted SiO_2 layers reveal only small differences between the RE profiles of the as-implanted state and devices annealed with FA 1,000°C (not shown).

As shown in Fig. 2.11, the picture changes in case of Eu. The implanted Eu profiles after FA 800°C and FLA 1,000°C look very similar to the as-implanted profile, while at FA 900°C or RTA 1,000°C 6 s, first agglomerations of Eu are visible at the SiO_2–SiON interface. Eu segregations at the Si–SiO_2 interface are not yet visible, but with increasing annealing temperature and/or annealing time, the Eu diffusion

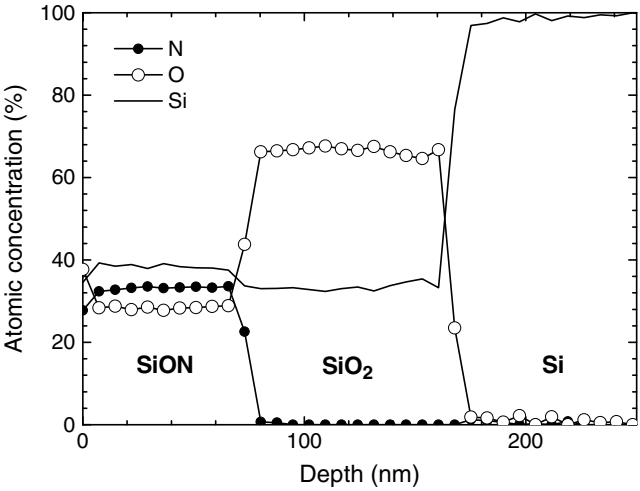

Fig. 2.9 Elemental composition of an unimplanted MOSLED annealed with RTA 1,000°C 6 s, as calculated from depth-dependent AES spectra obtained by sputtering

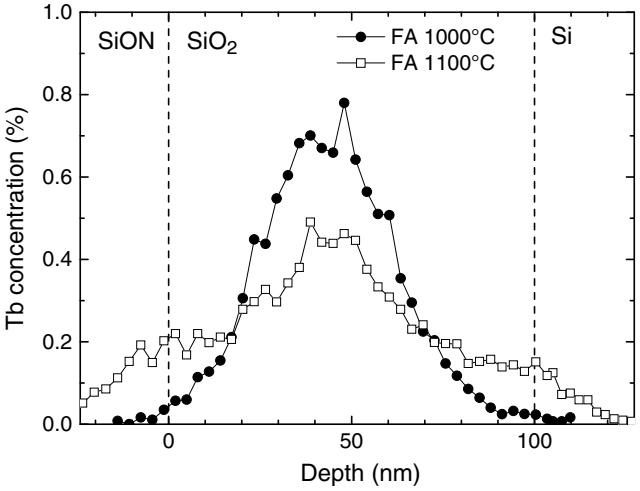

Fig. 2.10 Elemental depth profiles of Tb-implanted MOSLEDs, as calculated from RBS spectra. The implanted Tb dose from RBS was estimated to be about 2.2×10^{15} cm^{-2}

becomes more intense, and at FA 1,000°C, the amount of Eu at both interfaces is higher than in the middle of the oxide layer. If the middle of the oxide layer is defined as the region between 20 and 80 nm of the depth scale, as in Fig. 2.11, only 34% of the implanted Eu can be found within this region. This is even less than in the case of Tb implantation annealed by FA 1,100°C, where the central region still contains about 60% of the implanted Tb dose.

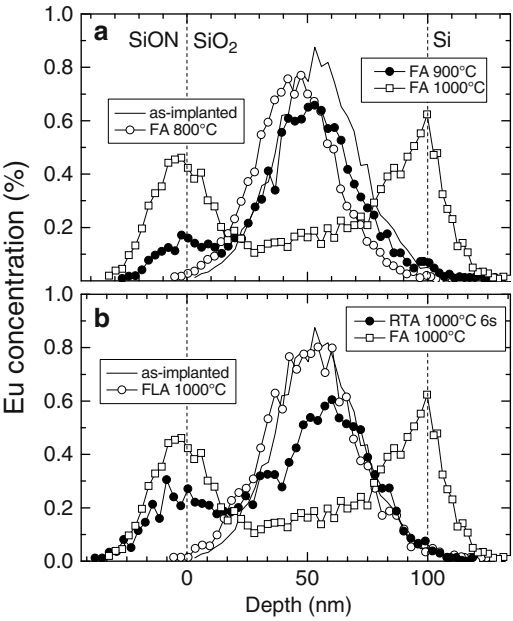

Fig. 2.11 Elemental depth profiles calculated from RBS spectra for Eu in SiO_2 layers implanted with a nominal dose of 3×10^{15} cm^{-2} and annealed with different annealing temperatures (**a**) and different annealing times (**b**). An atomic density of 6.6×10^{22} cm^{-3} has been assumed for the SiO_2 layer, to calculate the depth scale (after [132])

The RBS data imply that the diffusion of Eu is strongly enhanced compared with other RE elements. Unfortunately, to the best of our knowledge, no diffusion data of RE atoms in thermally grown SiO_2 can be found in the literature.

2.3 Cluster Formation and Growth

2.3.1 Morphology and Size Distribution

NC formation is a widespread phenomenon for material systems in which impurity atoms were incorporated in concentrations exceeding the solubility limit by far and which were subjected to annealing. Being related to ion-implanted MOSLEDs, the NC formation was investigated by TEM for Si- [182], Ge- [67, 183, 184] and Sn-implanted [185] SiO_2 layers. There are a few reports about clustering in RE-implanted SiO_2, with the majority dealing with Er [186]. According to the present state of knowledge, the cluster formation starts with the formation of ODCs as a result of the nuclear energy deposition during implantation (Sect. 2.2.1) and the deficiency of oxygen introduced by the RE ions. These ODCs serve as seeds for the formation of small clusters by nucleation, which can grow later in size by Ostwald ripening. If the thermal budget applied by annealing is sufficient, one or more cluster bands may arise, depending on the specific implantation and annealing conditions. A single implantation into the middle of the SiO_2 layer usually leads to

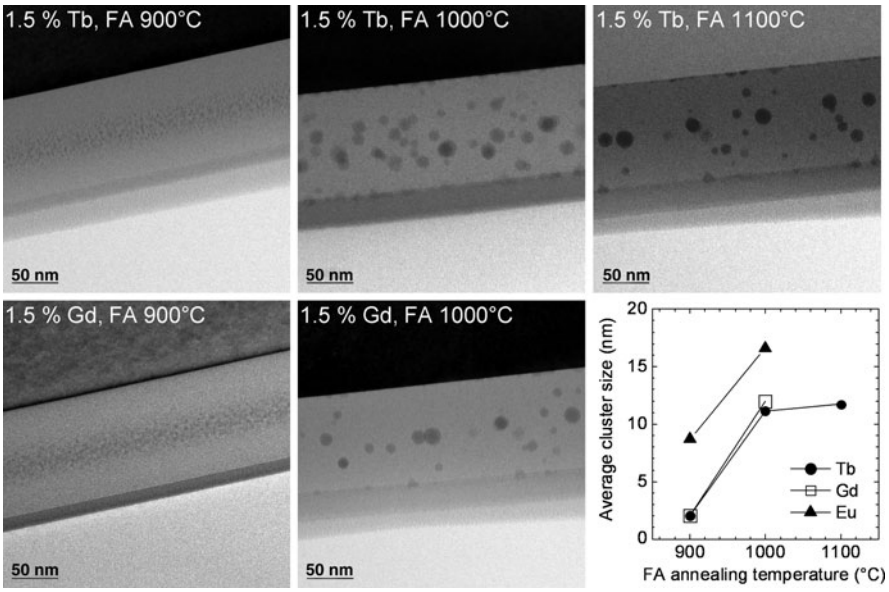

Fig. 2.12 TEM images from a SiO_2 layer single implanted with 1.5% of Tb and Gd furnace annealed between 900°C and 1,100°C (after [187]). The average cluster sizes are given in the *lower right corner*

the formation of a central cluster band with large and small clusters in the centre and the wings of the cluster band, respectively, whereas a double implantation can result in a broad cluster band with a narrow cluster size distribution [67]. Further morphologic features comprise the formation of a small and well-separated cluster band at the Si–SiO_2 interface [184], as well as the formation of cluster bands close to the SiO_2 surface as a consequence of the clash of two diffusion fronts [185].

Figure 2.12 displays a sequence of TEM images from MOSLEDs single implanted with Tb and Gd and annealed by FA between 900°C and 1,100°C. Starting from the top of the image, the bulk Si, a 100 nm thick SiO_2 layer containing the NCs, and a SiON layer with a thickness < 50 nm can be recognized. In case of 800°C (not shown), either no cluster (Tb) or very small clusters of 2 nm or less (Gd) can be observed [135]. At 900°C, both for Tb and Gd, small amorphous clusters with a mean size of about 2 nm are visible. This average size strongly increases to values around 11–12 nm if the annealing temperatures rise to 1,000°C, and first RE decorations at the Si–SiO_2 and the SiO_2–SiON interface can be recognized. A further increase of the annealing temperature to 1,100°C causes only a small increase in cluster size, but significantly more Tb is now found at the interfaces. The average cluster sizes for Tb, Gd and Eu (Fig. 2.13) are given in the graph in the lower right corner of Fig. 2.12.

Similar to the deviant RBS results for Eu (Sect. 2.2.3), the evolution of Eu or Eu oxide clusters differs from that of other RE elements too, as illustrated in Fig. 2.13

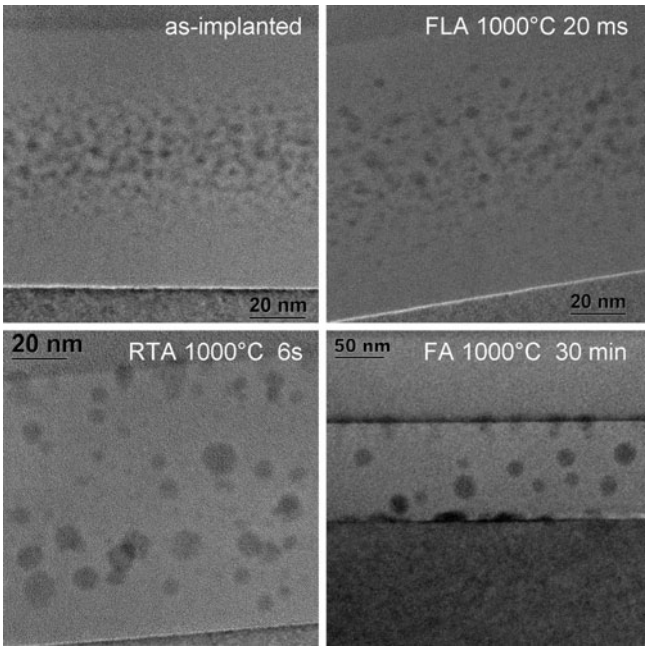

Fig. 2.13 Bright field XTEM images showing the gate oxide layer of Eu-implanted devices, together with its interfaces, to Si (*bottom*) and SiON (*up*). Please note the different magnification for FA 1,000°C (after [132])

showing a sequence of TEM images of Eu-implanted MOSLEDs in the as-implanted state and annealed at 1,000°C with increasing annealing time. The images exhibit the Eu-implanted SiO_2 layer with the adjacent Si substrate and the SiON layer at the bottom and the upper part of the images, respectively. Most noticeably, the cluster formation seems to be greatly accelerated compared with other RE elements. Thus, in the as-implanted state, small amorphous clusters with sizes of around 3–4 nm can already be found in the middle of the SiO_2 layer. As briefly discussed in the preceding chapter, this cluster formation is assumed to be caused by implantation-induced diffusion processes.

Although FLA 1,000°C does not change the picture very much, at RTA 1,000°C 6 s, the formation of larger clusters at the expense of smaller ones caused by Ostwald ripening can be observed. In addition, there is also a significant diffusion of Eu to the interfaces of the SiO_2 layer, which becomes evident by the first Eu segregations at the interfaces and by the broadened cluster band that now extends across the whole oxide layer. In the case of FA 1,000°C, the TEM images show large amorphous clusters up to 20 nm in size and SiO_2 interfaces that are heavily decorated with Eu. At the Si–SiO_2 interface, even the "dissolution" of large clusters can be observed.

A similar development is also found in the case of increasing annealing temperatures. In Fig. 2.14, the development of the cluster size distribution with increasing annealing time at 1,000°C is compared with the cluster development for FA with

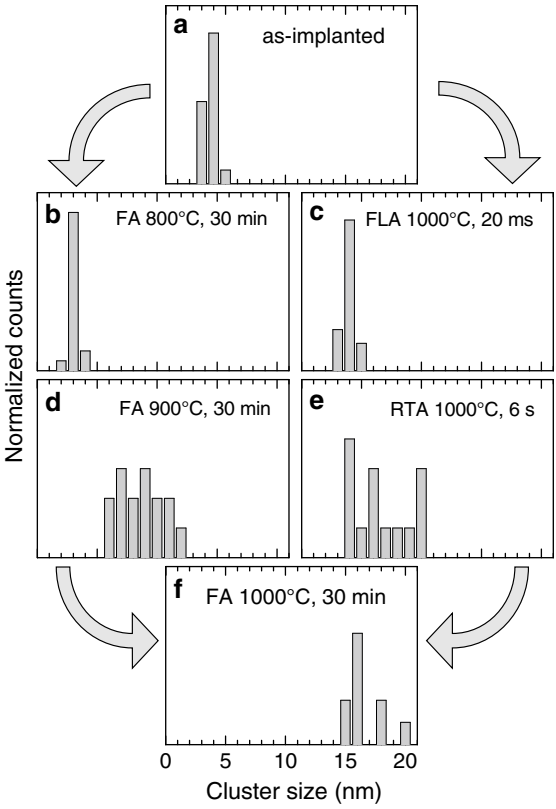

Fig. 2.14 Cluster size distribution of Eu/Eu oxide clusters as a function of the annealing temperature (*left column*) and the annealing time (*right column*). The cluster sizes were determined manually from the XTEM images shown in Fig. 2.13 (after [132])

increasing annealing temperature. Although the cluster sizes were determined manually from the TEM images, resulting in an uncertainty of 1–2 nm, the general tendency is obvious. If the thermal budget exceeds a certain limit either by high temperature or long annealing times, a strong Eu diffusion starts, which finally ends up with the structure known for FA 1,000°C with large Eu clusters and strong Eu segregations at the interfaces. The transition points, namely FA 900°C and RTA 1,000°C 6 s, appear to be equivalent. In the case of FA, the average cluster size is comparable with that of Tb and Gd-implanted devices in Fig. 2.12.

In summary, Eu seems to differ primarily from other RE elements, namely Gd, Tb and Er, because of its accelerated microstructural development, which is possibly caused by a higher diffusion in SiO_2. Consequently, other RE elements pass through the same development stages of morphology as Eu, but at higher thermal budgets. A strong RE diffusion towards the interfaces occurs even at 1,000°C for Eu, whereas at least 1,100°C is needed for the other RE elements (Figs. 2.10 and 2.11). In addition, the cluster sizes for Eu and FA 900°C seem to be similar to those

Table 2.1 Formation enthalpies of different RE oxides [188] and of amorphous SiO_2 at room temperature [189]

	Formation enthalpy (kJ mol^{-1})	Normalized formation enthalpy per reactant (kJ mol^{-1})
Eu_2O_3	−1,651.4	−825.7
Gd_2O_3	−1,819.6	−909.8
Tb_2O_3	−1,865.2	−932.6
Er_2O_3	−1,897.9	−948.95
SiO_2	−910	−910

of Tb and Gd at 1,000°C. However, although the TEM images and the RBS data corroborate the idea of an equal microstructural development with different velocities, it is not yet clear how far this model extends and if it also applies to the structure and composition of different RE clusters.

2.3.2 The Oxidation State of Rare Earth Clusters

RE elements are known to have the strong tendency to achieve a trivalent ionic configuration and to form an oxide, most probably RE_2O_3. This is illustrated in Table 2.1 showing the formation enthalpies of the corresponding RE oxides whose values are in the same order of magnitude than the SiO_2 value, if normalized to the reactant (one RE or one Si atom). As mentioned in Sect. 2.2.1, Si and oxygen are released from the SiO_2 network during the implantation. In the following phase of annealing (and even partly during the implantation), oxygen can be either reintegrated into the SiO_2 network or used to oxidize the RE atoms. There is a competition for oxygen between Si and the RE elements, and as a result the RE atoms will cluster as REO_x, with x depending on the supply and demand of oxygen. As the normalized formation enthalpies of RE_2O_3 except Eu_2O_3 are more negative (more exothermic) than that of SiO_2, and because of the higher demand on oxygen per Si atom, the available oxygen is favourably used to oxidize RE atoms.

At present, there are only a limited number of experimental indications for this scenario, which was described initially for Eu in [190]. In the rare case where crystalline clusters are observed in the TEM images of Eu-implanted MOSLEDs, the inter-planar spacing obtained by Fourier-transformation of the atomic planes of such crystallites confirms the formation of the Eu_2O_3 phase [132]. As the formation enthalpies of Gd_2O_3, Tb_2O_3 and Er_2O_3 are even more negative (more exothermic) than that of Eu_2O_3, these RE elements are also supposed to cluster in an oxidic form. The X-ray absorption fine structure analysis of Tb-implanted SiO_2 layers revealed that Tb is coordinated with either two or six oxygen atoms, and that the latter configuration is favoured by FA 900°C 30 min [191]. However, sixfold oxygen coordination strongly indicates a RE^{3+} configuration, and after FA 900°C 30 min, a major part of the Tb is bound in small clusters. In the case of Ce-rich SiO_2, it was reported that FA 1,200°C 3 h leads to the formation of $Ce_2Si_2O_7$ and related compounds [192]. A similar behaviour was observed for Pr, which formed $Pr_2Si_2O_7$ in Pr-rich SiO_2 after FA 1,100°C 1 h [193].

http://www.springer.com/978-3-642-14446-2

Rare-Earth Implanted MOS Devices for Silicon Photonics
Microstructural, Electrical and Optoelectronic Properties
Rebohle, L.; Skorupa, W.
2010, XVIII, 174 p. 120 illus., 3 illus. in color., Hardcover
ISBN: 978-3-642-14446-2